

Explore nuclearites in a large liquid scintillator neutrino detector

Wan-Lei Guo,^{1,*} Cheng-Jun Xia,^{2,†} Tao Lin,^{1,‡} and Zhi-Min Wang^{1,§}

¹*Institute of High Energy Physics, Chinese Academy of Sciences,*

P.O. Box 918, Beijing 100049, China

²*Key Laboratory of Theoretical Physics, Institute of Theoretical Physics,*

Chinese Academy of Sciences, Beijing 100190, China

Abstract

We take the JUNO experiment as an example to explore nuclearites in the future large liquid scintillator detector. Comparing to the previous calculations, the visible energy of nuclearites across the liquid scintillator will be reestimated for the liquid scintillator based detector. Then the JUNO sensitivities to the nuclearite flux are presented. It is found that the JUNO projected sensitivities can be better than $7.7 \times 10^{-17} \text{ cm}^{-2} \text{ s}^{-1} \text{ sr}^{-1}$ for the nuclearite mass $10^{15} \text{ GeV} \leq M \leq 10^{24} \text{ GeV}$ and initial velocity $10^{-4} \leq \beta_0 \leq 10^{-1}$ with a 20 year running. Note that the JUNO will give the most stringent limits for downgoing nuclearites with $1.6 \times 10^{13} \text{ GeV} \leq M \leq 4.0 \times 10^{15} \text{ GeV}$ and a typical galactic velocity $\beta_0 = 10^{-3}$.

PACS numbers: 14.80.-j, 21.65.-f, 95.55.Vj

*Electronic address: guowl@ihep.ac.cn

†Electronic address: cjxia@itp.ac.cn

‡Electronic address: lintao@ihep.ac.cn

§Electronic address: wangzhm@ihep.ac.cn

I. INTRODUCTION

Strange quark matter (SQM) is a hypothetical strongly interacting matter composed of roughly equal numbers of u , d , s quarks and a small amount of electrons [1, 2]. It is believed that SQM is the true ground state of quantum chromodynamics, where absolutely stable SQM objects with the baryon number A ranging from that of ordinary nuclei to neutron stars ($A \sim 10^{57}$) are expected [3]. The SQM has a little larger density than the saturation density of ordinary nuclear matter, which may be created in various situations, e.g., the hadronization process of the early universe [2], collision of binary compact stars [4, 5], type II supernovae driven by deconfinement phase transition [6], and even heavy ion collisions on Earth [7, 8]. The SQM objects are considered as the cold dark matter candidates and may be presented in the cosmic radiation reaching Earth. Light SQM objects ($A < 10^7$) are usually called strangelets [9–13], while in this work we focus on heavier ones ($M > 10^{10}$ GeV) known as nuclearites [14, 15]. Based on their special properties, the nuclearite searches have been performed by identifying the seismic activities with an epiliner source on Earth [16] and moon [17], the ionization tracks in ancient mica [18] and CR39 nuclear track detectors in the MACRO [19, 20], SLIM [21], and Ohya [22] experiments, the bar excitations induced by the thermo-acoustic effect in resonant bar detectors [23], the Rutherford backscattering of very heavy nuclei [24–26], the signatures of gravitational lensing caused by massive nuclearites [27, 28], and the photons emitted when a nuclearite moves through water in the ANTARES [29] experiment and atmosphere in the future JEM-EUSO [30] experiment, etc. Despite the non-observation of nuclearites, these experiments are able to constrain the upper limits on the flux of cosmic nuclearites.

The liquid scintillator (LS) as the detection medium in the past neutrino experiments has achieved great successes [31–34]. Now the next generation large LS detectors JUNO [35, 36] and LENA [37] are constructing in China and proposed in Europe, respectively. When a nuclearite passes through the LS medium, the elastic collisions between the nuclearite and ambient LS molecules will result in an over-heating track. Many photons from the black-body radiation of this track can be observed by the photomultiplier tubes (PMTs). Therefore the future large LS detectors have the ability to search for nuclearites. A major advantage of the LS detectors is that the LS wavelength shifters can absorb the short wavelength photons and reemit the longer wavelength photons. This feature ensures that the LS detectors can collect more photons from the black-body radiation of the nuclearite track. Here we shall take the JUNO detector as an exam-

ple to explore nuclearites. The JUNO is a 20 kton multi-purpose underground LS detector and primarily determines the neutrino mass hierarchy by detecting reactor antineutrinos. The JUNO detector is deployed in a 700 meter underground laboratory and consists of a central detector, a water Cherenkov detector and a muon tracker. The JUNO central detector holds 20 kton LS which will be in a spherical container with a radius of 17.7 m [35]. There is 1.5 m water buff region between about 18000 20-inch PMTs, 36000 3-inch PMTs and the LS surface.

In this paper, we shall explore nuclearites in the JUNO LS detector and analyze the JUNO detection capability. Comparing to the previous calculations, the visible energy of nuclearite per unit track length in the JUNO LS region will be reestimated in terms of the LS fluorescence quantum yields, the PMT quantum efficiencies and the JUNO detector design. Then we predict the JUNO sensitivities to the nuclearite flux. In Sec. II, we outline the main features of the nuclearite and give the maximal zenith angle below which nuclearites may pass through the Earth rocks and reach the JUNO detector. In Sec. III, the light yield of nuclearites traversing the JUNO LS will be analyzed in detailed. In Sec. IV, we present the JUNO sensitivity to the nuclearite flux based on some conditions. Finally, some discussions and conclusions will be given in Sec. V.

II. THE NUCLEARITE ENERGY LOSS

The dominant energy loss mechanism for nuclearites passing through matter is elastic or quasi-elastic collisions with the ambient atoms. As with meteorites, the nuclearite energy loss rate can be written as [14]

$$\frac{dE}{dx} = -\sigma\rho\beta^2, \quad (1)$$

where β is its velocity and ρ is the density of the traversed medium. The effective nuclearite cross section σ is given by

$$\sigma = \begin{cases} \pi R_0^2 = \pi(3M/4\pi\rho_N)^{2/3}; & M \geq 8.4 \times 10^{14} \text{ GeV}, \\ \pi \text{\AA}^2 = \pi \times 10^{-16} \text{ cm}^2; & M < 8.4 \times 10^{14} \text{ GeV}, \end{cases} \quad (2)$$

where the nuclearite density is estimated to be $\rho_N = 3.6 \times 10^{14} \text{ g}^{-1} \text{ cm}^{-3}$ [9] and the nuclearite radius R_0 can be easily induced from its mass M and density ρ_N . When the nuclearite radius $R_0 < 1 \text{\AA}$ ($M < 8.4 \times 10^{14} \text{ GeV}$), σ is dominated by the nuclearite electron atmosphere which is never smaller than the typical atomic size with the radius of $\sim 1 \text{\AA}$ [14, 38]. It is worthwhile to stress that the

right hand side of Eq. (1) should be replaced by the constant retarding force $-\varepsilon\sigma$ for the subsonic velocity $\beta < \beta_c = \sqrt{\varepsilon/\rho}$ with a structural energy density $\varepsilon \approx 10^9 \text{ erg cm}^{-3}$ [14].

Based on Eqs. (1) and (2), the travel length of a nuclearite depends on its mass M , velocity β and the medium density ρ . Some nuclearites may pass through the Earth rocks and arrive at the JUNO detector which has a 700 m rock overburden. For the JUNO detectable nuclearites, they will traverse different thickness of rocks based on their direction (zenith angle θ_z). In addition, one should consider the change of the Earth matter density. In terms of the PREM Earth density profile [39], we numerically calculate the maximal zenith angle θ_{\max} below which nuclearites may reach the JUNO detector, namely its local velocity $\beta_1 > 0$ at the detector level. The corresponding results have been plotted in Fig. 1 for $10^{12} \text{ GeV} \leq M \leq 10^{24} \text{ GeV}$ and 5 typical initial velocities β_0 at the ground level. It is clear that nuclearites from the $\theta_z = 0^\circ$ direction can reach the JUNO detector for $M > 10^{13} \text{ GeV}$ and $10^{-5} \leq \beta_0 \leq 10^{-1}$. For a typical galactic velocity $\beta_0 = 10^{-3}$, all directional nuclearites can arrive at the detector when $M > 2.5 \times 10^{22} \text{ GeV}$. Since the Earth density sharply changes between the core and mantle, we can see the knee points at $\theta_z = 146.9^\circ$ in Fig. 1.

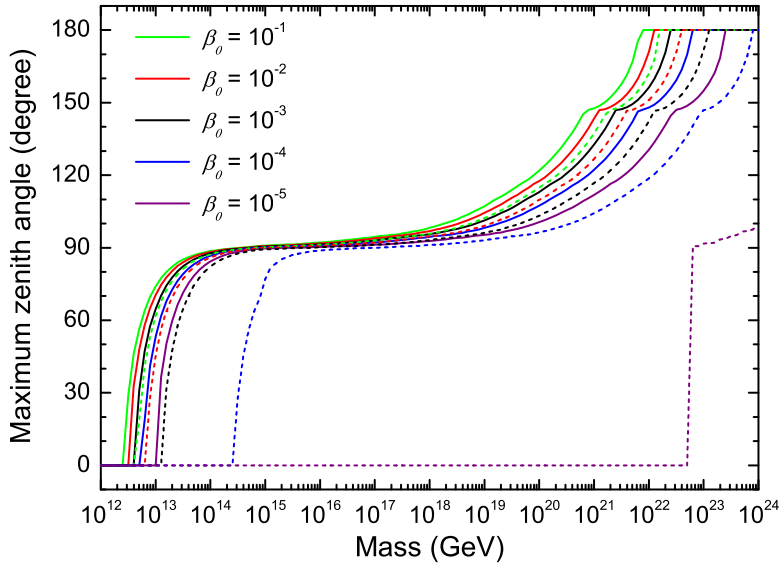


FIG. 1: The maximal zenith angles θ_{\max} below which the local velocity of nuclearite satisfies $\beta_1 > 0$ (solid lines) and $\beta_1 > \beta_{\min}$ (dashed lines) for 5 typical initial velocities β_0 at the ground level. In Sec. IV, we shall describe the minimal local velocity β_{\min} .

III. THE VISIBLE ENERGY OF NUCLEARITE IN JUNO LS

When a nuclearite traverses the JUNO LS medium, the LS molecules ($C_{18}H_{30}$) along the nuclearite path will disintegrate into their constituents because of the nuclearite elastic or quasi-elastic collisions. These heated atoms will further collide with the ambient LS molecules and generate a hot plasma shock wave [15]. The evolutions of effective temperature $T(t)$ and radius $R(t)$ of the expanding thermal shock wave can be written as [14]

$$R^2(t) = \sqrt{8}\beta_1 t R_0, \quad (3)$$

$$T(t) = m\beta_1 R_0 / (\sqrt{8}nt), \quad (4)$$

where m is the LS molecule mass and $n = 48$ is the number of submolecular species. Here β_1 denotes the local velocity of nuclearite at the detector level. The expanding cylindrical thermal shock wave can emit lights through the black-body radiation. The corresponding power spectrum is given by

$$\frac{dp}{d\omega da} = \frac{\hbar\omega^3}{4\pi^2 c^2} \frac{1}{e^{\hbar\omega/kT} - 1}, \quad (5)$$

where ω is the angular frequency and a denotes the area of shock wave. Then we can deduce the emitted photon numbers per unit track length dN_γ/dx from the expanding cylindrical shock:

$$\begin{aligned} \frac{dN_\gamma}{dx} &= \int d\omega \int dt 2\pi R(t) \frac{dp}{d\omega da} \frac{1}{\omega} \\ &= \frac{8^{\frac{1}{4}}}{2\pi} \sqrt{\beta_1 R_0} \int d\omega \int dt t^{\frac{1}{2}} \omega^2 \frac{1}{e^{\omega/T} - 1}, \end{aligned} \quad (6)$$

where we have used the natural system of units with $\hbar = c = k = 1$. Similarly, the total emitted energy dE_γ/dx can be directly obtained through the replacement $\omega^2 \rightarrow \omega^3$ in Eq. (6).

These emitted photons from the black-body radiation can not be entirely detected by the JUNO PMTs since they will suffer the absorption, re-emission and Rayleigh scattering processes in the JUNO LS [36]. On the other hand, the PMT quantum efficiency is related to the photon wavelength. Therefore one can not simply use the total emitted energy dE_γ/dx or the total photon numbers to describe the visible energy in the LS detector. It is convenient for us to calculate the visible energy if the photon electron (pe) efficiency per photon $\epsilon(\lambda)$ is available for the JUNO detector. Based on the LAB, PPO and bis-MSB fluorescence quantum yields [40], we adopt a combined PMT quantum efficiency curve shape from the Hamamatsu PMT data (400-800 nm) [41] and a fixed 27% efficiency (250-400 nm) to calculate $\epsilon(\lambda)$ for the wavelength range $250 \text{ nm} \leq \lambda \leq 800$

nm as shown in Fig. 2. We have assumed an averaged 60% survival probability of re-emitted photons from the detector center to the PMT surface and the 75% PMT photocathode coverage. It is found that the modeled $\epsilon(\lambda)$ approaches to zero for $\lambda > 640$ nm. In the absence of the related experimental data, we don't include the contribution of the $\lambda < 250$ nm case. Note that it will not significantly affect our final results.

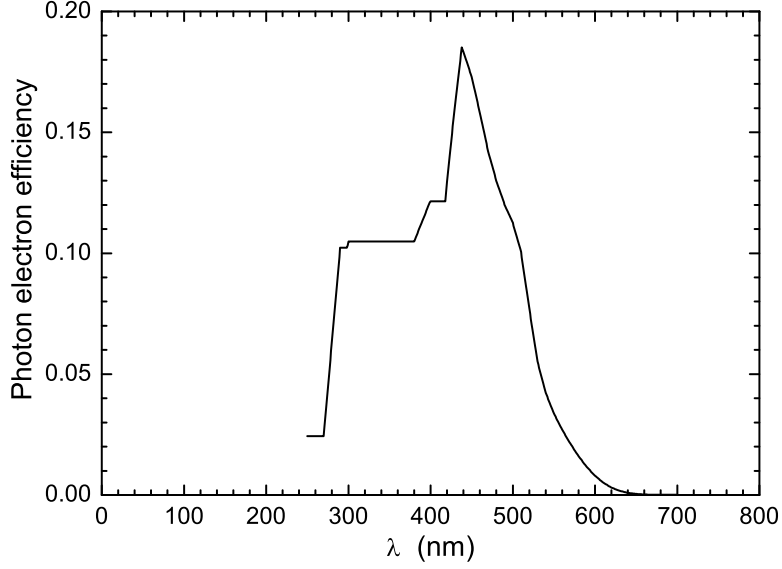


FIG. 2: The modeled photon electron efficiency per photon as a function of the wavelength λ .

With the help of Eq. (6) and the photon electron efficiency ϵ in Fig. 2, we can deduce the visible energy of nuclearite per unit track length in the JUNO LS:

$$\frac{dE_{vis}}{dx} = \frac{\text{MeV}}{1200\text{pe}} \frac{8^{\frac{1}{4}}}{2\pi} \sqrt{\beta_1 R_0} \int d\omega \omega^2 \epsilon(\omega) \int_{t_{\min}}^{\infty} dt t^{\frac{1}{2}} \frac{1}{e^{\omega/T} - 1}, \quad (7)$$

where t_{\min} takes the larger one of $t_0 = R_0/(\sqrt{8}\beta_1)$ and $t_1 = (l/R_0)^2 t_0$ [14] with the mean free path $l \approx 2.7\text{\AA}$. In Eq. (7), we have simply used that the 1 MeV gamma in the detector center may averagely produce 1200 photon electrons [35]. Based on Eq. (7), one may numerically calculate dE_{vis}/dx as shown in the left panel of Fig. 3. It is clear that dE_{vis}/dx does not vary for $M < 8.4 \times 10^{14}$ GeV. This is because we have adopted a constant value for R_0 in Eqs. (3) and (4), i.e., the radius of nuclearite electron atmosphere 1\AA . In the right panel of Fig. 3, we plot the ratio of dE_{vis}/dx and dE/dx as a function of the local nuclearite velocity β_1 . It is found that this ratio is independent of the nuclearite mass M when $M < 8.4 \times 10^{14}$ GeV and $M > 1.7 \times 10^{16}$ GeV. For the $M > 1.7 \times 10^{16}$ GeV case, namely $t_{\min} = t_0 > t_1$, one may easily find $dE_{vis}/dx \propto R_0^2$ through the variable substitution $t = t'R_0$.

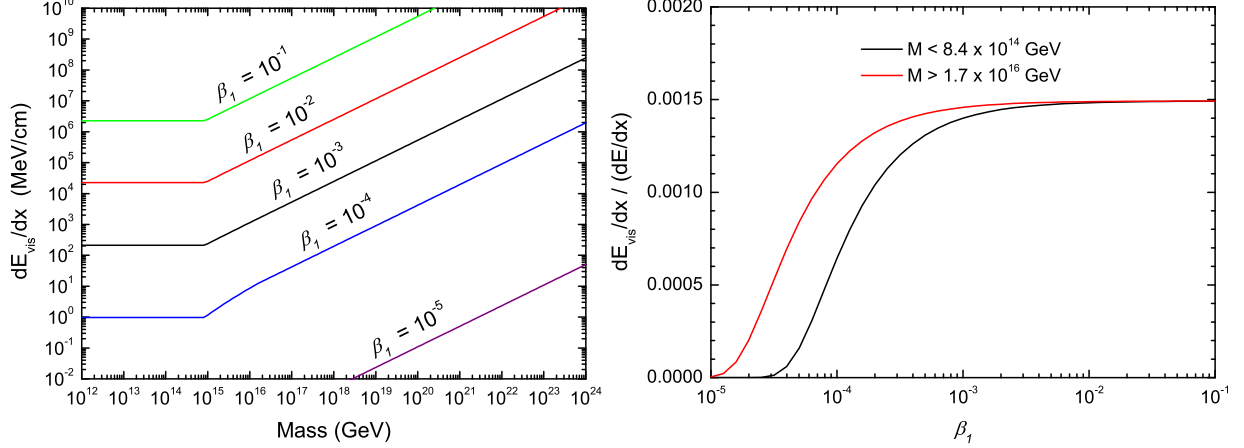


FIG. 3: Left panel: the visible energy of nuclearite per unit track length dE_{vis}/dx as a function of nuclearite mass for 5 typical β_1 ; Right panel: the ratio of dE_{vis}/dx and dE/dx as a function of β_1 .

IV. THE EXPECTED JUNO SENSITIVITIES

The light signals from nuclearites can be recorded when they satisfy the JUNO trigger conditions. Here we assume that the JUNO trigger threshold is 0.5 MeV within a 300 ns window for the following analyses. Then one may obtain

$$\beta_1 \times 300\text{ns} \times \frac{dE_{vis}}{dx} \geq 0.5 \text{ MeV} . \quad (8)$$

With the help of Eqs. (7) and (8), we calculate the minimal local velocity β_{\min} as shown in Fig. 4. It is clear that the local velocity β_1 must be larger than 8.7×10^{-6} for $10^{12} \text{ GeV} \leq M \leq 10^{24} \text{ GeV}$. For a fixed initial velocity β_0 at the ground level, the maximal zenith angle θ_{\max} can be deduced from Eq. (1) and the requirement $\beta_1 > \beta_{\min}$. In Fig. 1, we have plotted the corresponding θ_{\max} with dashed lines. It is found that the JUNO may detect all downgoing nuclearites (zenith angle $\theta_z < 90^\circ$) with $5.0 \times 10^{15} \text{ GeV} \leq M \leq 10^{24} \text{ GeV}$ and $10^{-3} \leq \beta_0 \leq 10^{-1}$. For the $\beta_0 = 10^{-5}$ case, the downgoing nuclearites with $M > 6.3 \times 10^{22} \text{ GeV}$ can satisfy the $\beta_1 > \beta_{\min}$ condition.

The expected nuclearite numbers in JUNO can be written as

$$N_S = 2\pi(1 - \cos \theta_{\max}) \phi T_{\text{run}} \pi R_{\text{eff}}^2 \quad (9)$$

where T_{run} is the JUNO running time and ϕ is the isotropic nuclearite flux in unit of $\text{cm}^{-2}\text{s}^{-1}\text{sr}^{-1}$. Here we require that the nuclearite track length in LS region should be larger than 5 m and derive the effective JUNO radius $R_{\text{eff}} = \sqrt{(17.7\text{m})^2 - (5\text{m}/2)^2} = 17.52 \text{ m}$. Then the 90% confidence level

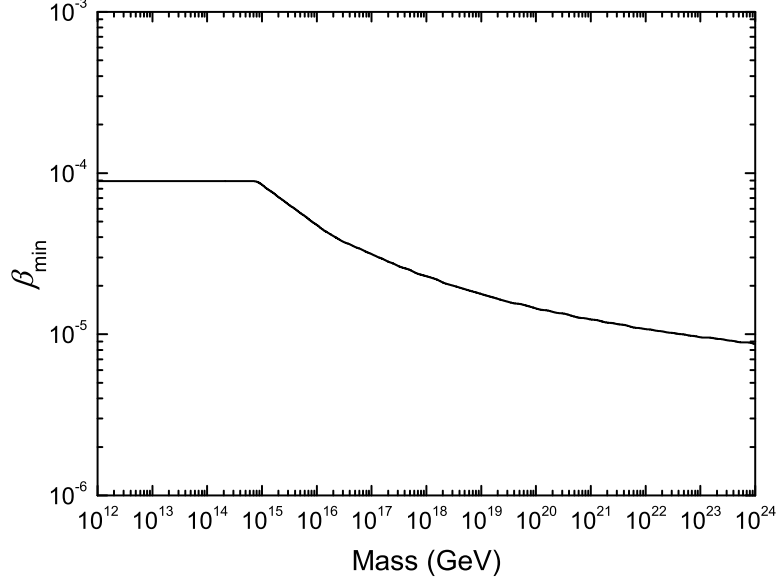


FIG. 4: The minimal local velocity β_{\min} above which nuclearites can satisfy the assumed JUNO trigger.

(CL) upper limit N_{90} to the expected N_S can be derived through the following formula [42, 43]:

$$90\% = \frac{\int_{N_S=0}^{N_{90}} L(N_{\text{obs}}|N_S) dN_S}{\int_{N_S=0}^{\infty} L(N_{\text{obs}}|N_S) dN_S} \quad (10)$$

with the Poisson-based likelihood function

$$L(N_{\text{obs}}|N_S) = \frac{(N_S + N_{BG})^{N_{\text{obs}}}}{N_{\text{obs}}!} e^{-(N_S + N_{BG})}. \quad (11)$$

To estimate the JUNO sensitivities to the nuclearite flux ϕ , we assume the background number $N_{BG} = 0$ and take the observed event number $N_{\text{obs}} = N_{BG} = 0$ for a 20 year running. With the help of Eqs. (9) and (10), we plot the 90% C.L. flux upper limits (solid lines) for 5 typical initial velocities β_0 as shown in the left panel of Fig. 5. It is clear that the JUNO sensitivities are better than $7.7 \times 10^{-17} \text{cm}^{-2} \text{s}^{-1} \text{sr}^{-1}$ for $10^{15} \text{ GeV} \leq M \leq 10^{24} \text{ GeV}$ and $10^{-4} \leq \beta_0 \leq 10^{-1}$. The JUNO is only sensitive to a narrow parameter space of the $\beta_0 = 10^{-5}$ case because of $\beta_1 < \beta_{\min}$. In addition, the most optimistic limit (black dotted line) has been also plotted for the $\beta_0 = 10^{-3}$ case where we only require $\beta_1 > 0$ and take $R_{\text{eff}} = 17.7 \text{ m}$.

To compare with the MACRO [20], ANTARES [29], SLIM [21] and Ohya [22] experimental results, we calculate the JUNO upper limit on the downgoing nuclearites in the $\beta_0 = 10^{-3}$ case. Our numerical results are presented in the right panel of Fig. 5. It is clear that the JUNO sensitivity is far better than the MACRO, SLIM and Ohya limits. Note that the JUNO will give the most stringent limit in the range of $1.6 \times 10^{13} \text{ GeV} \leq M \leq 4.0 \times 10^{15} \text{ GeV}$. In the most optimistic case

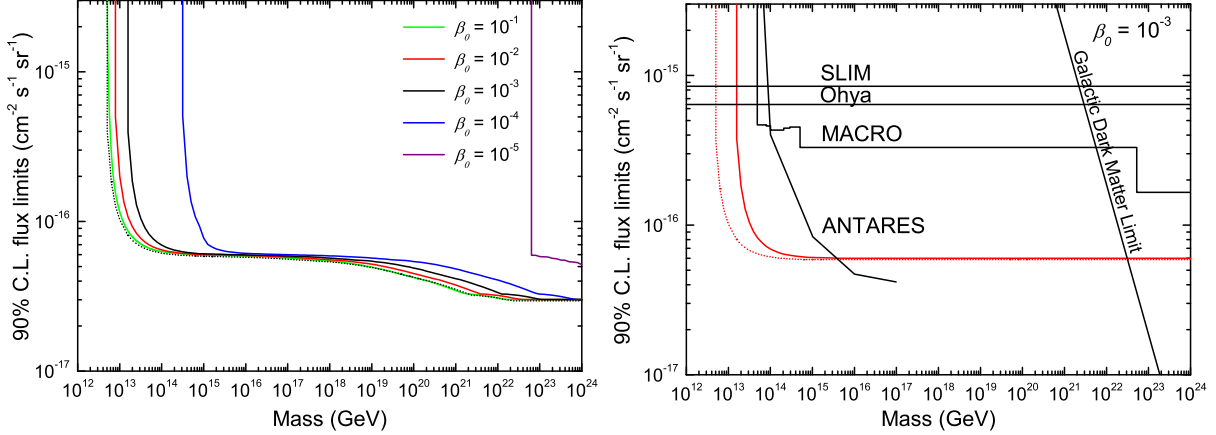


FIG. 5: The JUNO 90% C.L. flux upper limits to the all direction (left) and downgoing (right) nuclearites with the local velocity $\beta_1 > \beta_{\min}$ and the effective LS radius $R_{\text{eff}} = 17.52$ m for a 20 year running. The black and red dotted lines describe the JUNO most optimistic limits with $\beta_1 > 0$ and $R_{\text{eff}} = 17.7$ m in the initial velocity $\beta_0 = 10^{-3}$ case.

(red dotted line), the above range can be extended to $5.0 \times 10^{12} \text{ GeV} \leq M \leq 4.0 \times 10^{15} \text{ GeV}$. Here we have also plotted the galactic dark matter (DM) upper limit $\phi_{\text{max}} = \rho_{\text{DM}}\beta_0/(2\pi M)$ [14, 20] where nuclearites are assumed to contribute all of the local DM density $\rho_{\text{DM}} = 0.39 \text{ GeV cm}^{-3}$ [44]. For $M > 3.1 \times 10^{22} \text{ GeV}$, the galactic DM limit is dominant. In future, the JEM-EUSO experiment will give a more stringent limit $\phi < 10^{-20} \text{ cm}^{-2} \text{ s}^{-1} \text{ sr}^{-1}$ for $M > 5 \times 10^{22} \text{ GeV}$ [30].

V. DISCUSSIONS AND CONCLUSIONS

As mentioned in Sec. III, the photon electron efficiency per photon $\epsilon(\lambda)$ is not considered for the $\lambda < 250 \text{ nm}$ range because of the absence of the related experimental data. If these data are available in future, we shall derive the larger dE_{vis}/dx than those in the left panel of Fig. 3. Then the smaller β_{\min} will be expected. The predicted sensitivities (solid lines from $\beta_1 > \beta_{\min}$) in Fig. 5 will approach to the most optimistic limits (the corresponding dotted lines from $\beta_1 > 0$). It is clear that our results don't change significantly for $M > 1.0 \times 10^{14} \text{ GeV}$ and $\beta_0 = 10^{-3}$. Note that the nuclearite mass can't be correctly reconstructed from the incomplete $\epsilon(\lambda)$ when a nuclearite is really detected by the JUNO LS detector. In addition, the JUNO can only give the mass lower bound for very large dE_{vis}/dx because of the PMT saturation.

In conclusion, we have investigated nuclearites in the JUNO LS detector. Comparing to the previous calculations, the visible energy of nuclearite in the LS has been estimated in detail. Then

we give the JUNO detectable range of zenith angle for the nuclearite mass $10^{12} \text{ GeV} \leq M \leq 10^{24} \text{ GeV}$ and five typical initial velocities β_0 at the ground level. Finally, we present the JUNO sensitivities to the nuclearite flux for a 20 year running. It is found that the JUNO sensitivities to all directional nuclearites are better than $7.7 \times 10^{-17} \text{ cm}^{-2} \text{ s}^{-1} \text{ sr}^{-1}$ for $10^{15} \text{ GeV} \leq M \leq 10^{24} \text{ GeV}$ and $10^{-4} \leq \beta_0 \leq 10^{-1}$. For the downgoing nuclearites, the expected sensitivities are much better than those from the MACRO, SLIM and Ohya experiments in the case of $\beta_0 = 10^{-3}$. Note that the JUNO will give the most stringent limits for $1.6 \times 10^{13} \text{ GeV} \leq M \leq 4.0 \times 10^{15} \text{ GeV}$.

Acknowledgments

We are grateful to Jun Cao, Liang Zhan and Shan-Gui Zhou for their very useful discussions and critical remarks. This work is supported in part by the National Nature Science Foundation of China (Grant Nos. 11525524, 11575201 and 11621131001), and the Strategic Priority Research Program of the Chinese Academy of Sciences under Grant No. XDA10010100.

-
- [1] A. R. Bodmer, Phys. Rev. D **4**, 1601 (1971). doi:10.1103/PhysRevD.4.1601
 - [2] E. Witten, Phys. Rev. D **30**, 272 (1984). doi:10.1103/PhysRevD.30.272
 - [3] C. J. Xia, G. X. Peng, E. G. Zhao and S. G. Zhou, Phys. Rev. D **93**, no. 8, 085025 (2016). doi:10.1103/PhysRevD.93.085025
 - [4] J. Madsen, J. Phys. G **28**, 1737 (2002) doi:10.1088/0954-3899/28/7/327 [hep-ph/0112153].
 - [5] A. Bauswein, H.-T. Janka, R. Oechslin, G. Pagliara, I. Sagert, J. Schaffner-Bielich, M. M. Hohle and R. Neuhauser, Phys. Rev. Lett. **103**, 011101 (2009) doi:10.1103/PhysRevLett.103.011101 [arXiv:0812.4248 [astro-ph]].
 - [6] H. Vucetich and J. E. Horvath, Phys. Rev. D **57**, 5959 (1998) doi:10.1103/PhysRevD.57.5959 [astro-ph/9802363].
 - [7] K. Borer *et al.*, Phys. Rev. Lett. **72**, 1415 (1994). doi:10.1103/PhysRevLett.72.1415
 - [8] R. M. Weiner, Int. J. Mod. Phys. E **15**, 37 (2006) doi:10.1142/S0218301306004004 [hep-ph/0507115].
 - [9] S. A. Chin and A. K. Kerman, Phys. Rev. Lett. **43**, 1292 (1979). doi:10.1103/PhysRevLett.43.1292
 - [10] E. Farhi and R. L. Jaffe, Phys. Rev. D **30**, 2379 (1984). doi:10.1103/PhysRevD.30.2379
 - [11] M. S. Berger and R. L. Jaffe, Phys. Rev. C **35**, 213 (1987). doi:10.1103/PhysRevC.35.213

- [12] E. P. Gilson and R. L. Jaffe, Phys. Rev. Lett. **71**, 332 (1993) doi:10.1103/PhysRevLett.71.332 [hep-ph/9302270].
- [13] G. X. Peng, X. J. Wen and Y. D. Chen, Phys. Lett. B **633**, 314 (2006) doi:10.1016/j.physletb.2005.11.081 [hep-ph/0512112].
- [14] A. De Rujula and S. L. Glashow, Nature **312**, 734 (1984). doi:10.1038/312734a0
- [15] A. De Rujula, Nucl. Phys. A **434**, 605C (1985). doi:10.1016/0375-9474(85)90525-1
- [16] E. T. Herrin, D. C. Rosenbaum and V. L. Teplitz, Phys. Rev. D **73**, 043511 (2006) doi:10.1103/PhysRevD.73.043511 [astro-ph/0505584].
- [17] W. B. Banerdt, T. Chui, E. T. Herrin, D. Rosenbaum and V. L. Teplitz, Adv. Space Res. **37**, 1889 (2006). doi:10.1016/j.asr.2005.06.034
- [18] P. B. Price, Phys. Rev. D **38**, 3813 (1988). doi:10.1103/PhysRevD.38.3813
- [19] S. P. Ahlen *et al.* [MACRO Collaboration], Phys. Rev. Lett. **69**, 1860 (1992). doi:10.1103/PhysRevLett.69.1860
- [20] M. Ambrosio *et al.* [MACRO Collaboration], Eur. Phys. J. C **13**, 453 (2000) doi:10.1007/s100520050708 [hep-ex/9904031].
- [21] S. Cecchini *et al.* [SLIM Collaboration], Eur. Phys. J. C **57**, 525 (2008) doi:10.1140/epjc/s10052-008-0747-7 [arXiv:0805.1797 [hep-ex]].
- [22] S. Orito *et al.*, Phys. Rev. Lett. **66**, 1951 (1991). doi:10.1103/PhysRevLett.66.1951
- [23] P. Astone *et al.*, arXiv:1306.5164 [astro-ph.HE].
- [24] J.-G. Lv, S.-J. Liu, N.-Q. Liu, Y.-Q. Li, H.-T. Li, S.-Y. Song, Y. Wu, R.-S. Wu, T.-B. Zhang, P.-Y. Zheng, *et al.*, Prog. Phys. **9**, 385 (1988), in Chinese, URL <http://www.cnki.com.cn/Article/CJFDTOTAL-WLXJ198904000.htm>
- [25] S.-J. Liu, B.-Z. Xie, Y. Wu, and X.-W. Tang, High Energ. Phys. Nuc. **13**, 103 (1989), in Chinese, URL <http://www.cnki.com.cn/Article/CJFDTotal-KNWL198902001.htm>
- [26] D. M. Lowder, Nucl. Phys. Proc. Suppl. **24B**, 177 (1991). doi:10.1016/0920-5632(91)90321-5
- [27] A. Barnacka, J. F. Glicenstein and R. Moderski, Phys. Rev. D **86**, 043001 (2012) doi:10.1103/PhysRevD.86.043001 [arXiv:1204.2056 [astro-ph.CO]].
- [28] K. Griest, A. M. Cieplak and M. J. Lehner, Astrophys. J. **786**, no. 2, 158 (2014) doi:10.1088/0004-637X/786/2/158 [arXiv:1307.5798 [astro-ph.CO]].
- [29] G. E. Pavalas [ANTARES Collaboration], PoS ICRC **2015**, 1060 (2016).
- [30] M. Bertaina *et al.* [JEM-EUSO Collaboration], Exper. Astron. **40**, no. 1, 253 (2015).

doi:10.1007/s10686-014-9375-4

- [31] C. L. Cowan, F. Reines, F. B. Harrison, H. W. Kruse and A. D. McGuire, *Science* **124**, 103 (1956).
doi:10.1126/science.124.3212.103
- [32] K. Eguchi *et al.* [KamLAND Collaboration], *Phys. Rev. Lett.* **90**, 021802 (2003)
doi:10.1103/PhysRevLett.90.021802 [hep-ex/0212021].
- [33] C. Arpesella *et al.* [Borexino Collaboration], *Phys. Rev. Lett.* **101**, 091302 (2008)
doi:10.1103/PhysRevLett.101.091302 [arXiv:0805.3843 [astro-ph]].
- [34] F. P. An *et al.* [DAYA-BAY Collaboration], *Phys. Rev. Lett.* **108**, 171803 (2012) [arXiv:1203.1669
[hep-ex]].
- [35] F. An *et al.* [JUNO Collaboration], *J. Phys. G* **43**, no. 3, 030401 (2016) doi:10.1088/0954-
3899/43/3/030401 [arXiv:1507.05613 [physics.ins-det]].
- [36] Z. Djurcic *et al.* [JUNO Collaboration], arXiv:1508.07166 [physics.ins-det].
- [37] M. Wurm *et al.* [LENA Collaboration], *Astropart. Phys.* **35**, 685 (2012)
doi:10.1016/j.astropartphys.2012.02.011 [arXiv:1104.5620 [astro-ph.IM]].
- [38] D. Bakari *et al.*, hep-ex/0004019.
- [39] A. M. Dziewonski and D. L. Anderson, *Phys. Earth Planet. Inter.* **25**, 297 (1981).
- [40] C. Buck, B. Gramlich and S. Wagner, *JINST* **10**, no. 09, P09007 (2015) doi:10.1088/1748-
0221/10/09/P09007 [arXiv:1509.02327 [physics.ins-det]].
- [41] http://www.hamamatsu.com/resources/pdf/etd/PMT_TPMZ0002E.pdf
- [42] T. Tanaka *et al.* [Super-Kamiokande Collaboration], *Astrophys. J.* **742**, 78 (2011) [arXiv:1108.3384
[astro-ph.HE]].
- [43] W. L. Guo, Z. L. Liang and Y. L. Wu, *Nucl. Phys. B* **878**, 295 (2014) [arXiv:1305.0912 [hep-ph]];
W. L. Guo, *JCAP* **1601**, no. 01, 039 (2016) doi:10.1088/1475-7516/2016/01/039 [arXiv:1511.04888
[hep-ph]].
- [44] K. A. Olive *et al.* [Particle Data Group Collaboration], *Chin. Phys. C* **38**, 090001 (2014).
doi:10.1088/1674-1137/38/9/090001